5-2019

The Effects of Starspots and Faculae on the G-band, Ca I, and Hγ Photospheric Indices

David Cameron McCallister
University of Tennessee, dmccall2@vols.utk.edu

The Effects of Starspots and Faculae on the G-band, Ca I, and Hγ Photospheric Indices

A Thesis Presented for the

Master of Science

Degree

The University of Tennessee, Knoxville

David Cameron McCallister

May 2019

For Joseph Dale Perry, who turned his telescope up into the dark West Virginia skies and gave his grandson a passion for science and a life-long love of astronomy.

.

For David Alan McCallister, whose paternal lessons on perseverance echoed strongly in my mind when I thought about giving up.

.

For Joseph Jordan McCallister, who is loved beyond measure, and who blessed us by arriving a week after this thesis was defended.

Acknowledgments

This project could not have been completed without help from many people. My wife's support throughout my returning to higher education has been both rock steady and essential. I would like to thank the University of Tennessee Physics and Astronomy Department, in particular Dr. Hanno Weitering and Dr. Marianne Breinig, for allowing me to pursue this observational astronomy topic that called for working outside the department's research professors. As a graduate student, I won the lottery in terms of the supportive advisors that I have had during my time pursuing this master's degree. I had the unique opportunity to be the first master's advisee of Dr. Sean Lindsay, who could not have been more supportive. For the many times you gently guided me back on track, thank you. Appalachian State University's Dr. Richard Gray has also been very generous with his time and guidance. In addition, I would like to thank my thesis committee for their helpful comments and suggested revisions: Dr. Michael Guidry, Dr. Raph Hix, and Dr. Andrew Steiner. I also gratefully acknowledge the use of NASA's Astrophysics Data System Bibliographic Services, and the University of Tennessee Knoxville Graduate School's LaTeX template for master's theses.

Abstract

The observation and analysis of solar-type stars has been a rich area of research. Determining what the Sun was like when life was first taking hold on Earth, and what the Sun will be like as it ages with the potential impacts on the future Earth, provides the motivation for a number of monitoring campaigns to photometrically and spectroscopically measure collections of solar-like stars (solar analogs). One such campaign, The Young Solar Analogs (YSA) Project, has been monitoring 30 stars in the range of ages 300 million to 1.5 billion years old, and spectral classes F8 - K2 [10]. The focus of this thesis is the creation and implementation of a computational model for the photospheres of the YSA program stars. I analyze the links between the photospheric features on a model star and the rotational modulation of photometric flux in the Johnson-Cousins B, V, and R bands, as well as spectroscopic indices derived from the G Band, Hγ, and Ca I photospheric features. This project constructs a computer model of stellar photospheres built on ATLAS9 models and the SPECTRUM spectral synthesis code that models rotational modulation of stars due to stellar spots. This paper presents preliminary results that show that the variations in the photospheric indices found by Gray et al. cannot be explained solely by faculae and star spots.

Table of Contents

List of Tables

List of Figures

Chapter 1

Background

1.1 Introduction

Since 2008, the Young Solar Analogs (YSA) project has been monitoring 30 main sequence stars between 0.3 and 1.5 billion years old in an effort to determine what our young Sun was like around the time life was starting on Earth. As a part of this effort, the Dark Sky Observatory (DSO) run by Appalachian State University has been collecting spectra in the blue-violet region of the spectrum and photometry in the Johnson-Cousins B, V, and R bands.

Monitoring the changes in a star's chromosphere is a proxy for stellar activity. The first paper in the YSA project, Gray et al. (2015) introduced three new photospheric indices based on the G-band, Hγ, and Ca I photospheric absorption features [10]. These indices were developed to track temperature changes related to stellar activity in the photospheres of the YSA program stars. However, their analysis showed unexpected correlations that suggested the presence of non-thermal effects.

This thesis focuses on the relationship between changes in the photometric magnitudes in the Johnson-Cousins B, V, and R bands and photospheric indices of Gray et al. Specifically, the hypothesis of this thesis is that the changes in these indices as measured by Gray et al. can be explained solely by temperature changes due to spot and facular coverage. This hypothesis will be tested by creating model photospheres, tuning the umbra, penumbra,

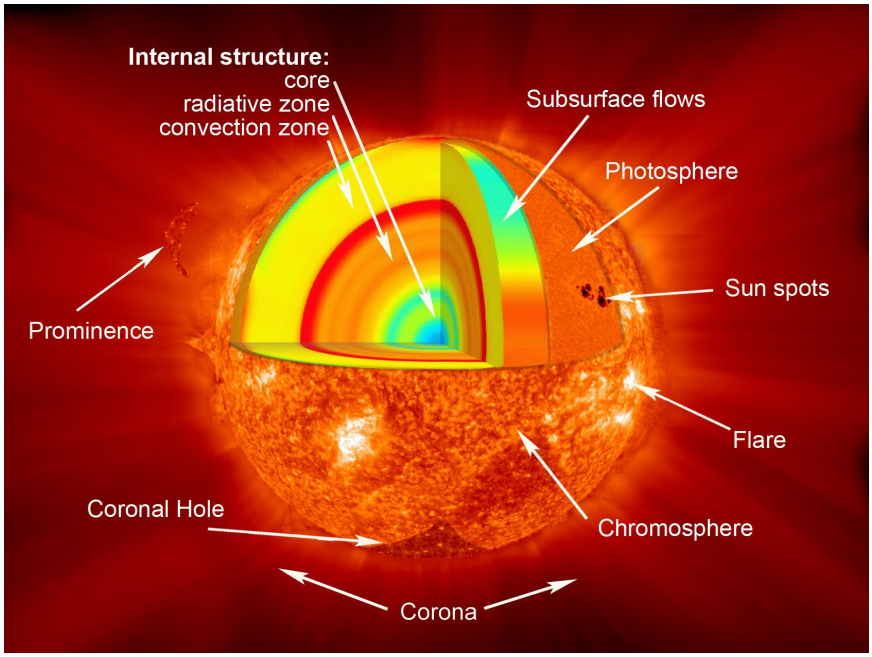

Figure 1.1: A cutaway of the sun. NASA.

and facula radii to match the modulation of the observed Johnson-Cousins B, V, and R photometry, then analyzing the modulations of the photospheric indices.

Due to computational constraints, model photospheres are one dimensional (depth) with plane parallel symmetry and local thermodynamic equilibrium, making it a challenge to model spots. This project develops a computer code that synthesizes a model star photosphere using a 2D grid consisting of 1D model photospheres. This makes it possible to introduce non-homogeneities (spots and faculae) on the stellar surface. The code adjusts the spot and facular size until the computed variations match the observed modulations in the Johnson-Cousins B, V, and R photometry. The same optimized model is used to compute the modulations in the photospheric (G-band, Hγ, and Ca I) indices which are then compared to the observed modulations.

1.2 Stellar Photospheres

The most extensively studied star is our own Sun. By observing the dark spots moving across the solar disk, Galileo was able to determine the rotation rate of the sun, as well as determine that the spots lie close to the "solar surface." We now describe this layer as the

photosphere, the layer from which nearly all photons leave the sun, where photons undergo their last few, critical interactions before leaving. The photosphere of our sun is only about 400 kilometers thick, compared to a solar radius of 696,000 km. Scaling this to the Earth's radius of 6,370 km, the photosphere would extend only 12 feet above the Earth's surface. It is this razor thin nature of the photosphere that results in a crisp, well-defined boundary seen when the Sun is viewed at visible wavelengths.

The interior of a star is composed of plasma that is nearly completely ionized and interacts with the radiation field through absorption and emission by ions, including electron scattering and free-free and bound-free interactions. Through a series of these interactions, a gamma-ray photon produced in the core becomes hundreds of lower energy photons on its way to the surface. In the high-density interior, the mean free path, or average distance between collisions with a gas molecule, is short, which means that collisions couple the radiation field to the thermal state of the gas. This condition allows a nearly perfect state of thermodynamic equilibrium, and so this material may be modeled as a blackbody radiator. Owing to the reduced density, the mean free path in the photosphere is significantly longer than in the stellar interior. Because of this, the local state of the gas and the emergent radiation field are not necessarily strongly coupled. However, the pressures and densities in the photospheres of main sequence stars are sufficiently high that the assumption of local thermodynamic equilibrium remains reasonable.

1.2.1 Effective Temperature

The luminosity or total power output of a spherical blackbody radiator is given by the Stefan-Boltzmann law,

$$L = 4\pi R^2 \sigma_{\mathrm{SB}} T^4$$

where L is the luminosity of the blackbody radiator, R its radius, and T its temperature. Even though a star is not a perfect blackbody radiator, we can define a blackbody equivalent temperature (the effective temperature, T_{eff}) given by

$$T_{\mathrm{eff}} = \left(\frac{L}{4\pi R^2 \sigma_{\mathrm{SB}}} \right)^{1/4}$$

The effective temperature corresponds roughly to the layer in the photosphere with an optical depth of 2/3. It is at this layer that the stellar continuum is formed. For the model photosphere in this thesis, the non-spot areas of the stellar disk were modelled as a photosphere with an effective temperature equal to the effective temperature of the star.

1.2.2 Radiative Transfer Equation

In order to model the photosphere of a star, the transfer of radiation through the photosphere must be modelled. The energy dE_ν per unit frequency, through solid angle $d\omega$ and time dt from a source of specific intensity I_ν observed at position $\vec{r}$, at frequency ν, in direction $\vec{n}$, at time t is given by the following equation:

$$dE_\nu = I_\nu(\vec{r}, \vec{n}, t)\, d\nu\, d\omega\, dt\, \mu dA \tag{1.1}$$

where μ is defined as the cosine of the angle between the normal to the area element dA and viewing direction n. Specific intensity is conserved along a ray, so the only changes to this quantity over a path length s are due to emission and absorption, which can be characterized by

$$\mu\, dI_\nu(s) = j_\nu(s)ds - \alpha_\nu(s)\, I_\nu(s)ds \tag{1.2}$$

where $j_\nu(s)$ is the emission coefficient and $\alpha_\nu(s)$ is the absorption coefficient. The optical depth is defined by $d\tau_\nu = -\alpha_\nu(s)ds$, so that $\tau_\nu = \int_0^s \alpha_\nu(s)ds$. If the medium is homogeneous along s such that the absorption coefficient does not change, then this reduces to $\tau_\nu = \alpha s$. This allows us to rewrite the above in terms of a source function $S_\nu = \frac{j_\nu}{\alpha_\nu}$:

$$\mu\frac{dI_\nu}{d\tau_\nu} = S_\nu - I_\nu \tag{1.3}$$

Equation 1.3 is known as the equation of radiative transfer. The source function is a characterization of the emission and absorption at a particular wavelength in the radiation field. Where local thermodynamic equilibrium can be assumed, the incident radiation can

be considered a blackbody, and the source function is given by Planck's function at the local temperature.

1.2.3 Spots

Because the regions around sunspots exhibit Zeeman splitting, sunspots are known to be a manifestation of local enhancements in the magnetic field of the sun. This suppresses the local convective energy transport causing spots to be cooler than the surrounding photosphere. Four hundred years of sunspot observations dating back to Galileo reveal a cycle of increasing and decreasing sunspot numbers with a period of about 11 years on the average. Other aspects of 'solar activity', including solar flares and Coronal Mass Ejections (CMEs) are correlated with sunspot number. A spot consists of an umbra, centrally located and dark compared to the rest of the photosphere due to being over 1000 K cooler, and a penumbra, which surrounds the umbra, is brighter than the umbra, but is not as bright as the rest of the photosphere. Penumbra are typically a few hundred kelvins cooler than the surrounding photosphere. In our model photosphere, spots will be modelled as local temperatures that are lower than the surrounding effective temperature, 1600 K lower for the umbra and 300 K lower for the penumbra.

1.2.4 Faculae

When the sun is viewed in high angular resolution photography, the photosphere is seen to be made up of Texas-sized convection cells called granules. Hot gas rises in the center, cools, and sinks back down the sides of the granule. Faculae are pockets of hydrogen gas that form between granules and are brighter than the photosphere. Facular density is correlated with the number of sunspots in the photosphere. Even when dark spots transit the sun, the faculae can compensate for the lack of flux due to sunspots and even increase total solar irradiance (TSI) [3].

This thesis uses two different facular models. The "Solid Halo" model, in which there is a solid ring of faculae around the penumbra at 100 K above the effective temperature, and the "Sprinkled In" model, in which faculae at 300 K above the effective temperature

are randomly placed with a filling factor of 0.3. The hypothesis of this thesis is that the temperature variations from spots and faculae are sufficient to explain the variations in the photospheric indices and their correlations with Johnson - Cousins B, V, and R photometry observed by Gray et al.

1.2.5 Limb Darkening

Limb darkening in the photosphere occurs because the optical depth reaches a value of 1 at a higher altitude near the limb as opposed to the center of the stellar disk. Since the temperature of this layer is cooler, the light around the edge of the sun is less intense than the light coming from the center. Since we are modelling spots as they transit across the sun, we must account for limb darkening effects. The specific intensity mode of the SPECTRUM code (Section 2.2) allows for the calculation of the emergent intensity spectrum at any point on the solar disk, given a direction cosine (μ).

1.3 Stellar Chromospheres

George Airy was the first to describe the Sun's chromosphere in 1851 after observing a total solar eclipse. Seeing small prominences giving it a jagged appearance, he mistook it for mountains and called it the "sierra". J. Norman Lockyer coined the moniker chromosphere to describe the pink ring of emission at the solar limb in 1868, citing the red color of the "flames" we now call prominences [14]. A simple definition of the chromosphere is that it is a layer 2000 to 3000 km thick, above the photosphere of the star. However, Jeffrey Hall notes that the chromosphere is not so well-defined, calling it "extremely inhomogeneous, variable on short and long timescales, and characterized by strongly confined and directed regions of hot plasma that suggest a complicated magnetic topology [11]." It is this activity that makes the assumption of local thermodynamic equilibrium for our model star break down, and why the chromosphere is not easily modelled. The magnetic forces that drive the "stellar activity" of a star also dynamically change the chromosphere. Lockwood et al. notes "chromospheric activity produces a stronger and more easily detected signal than photometric variability [13]."

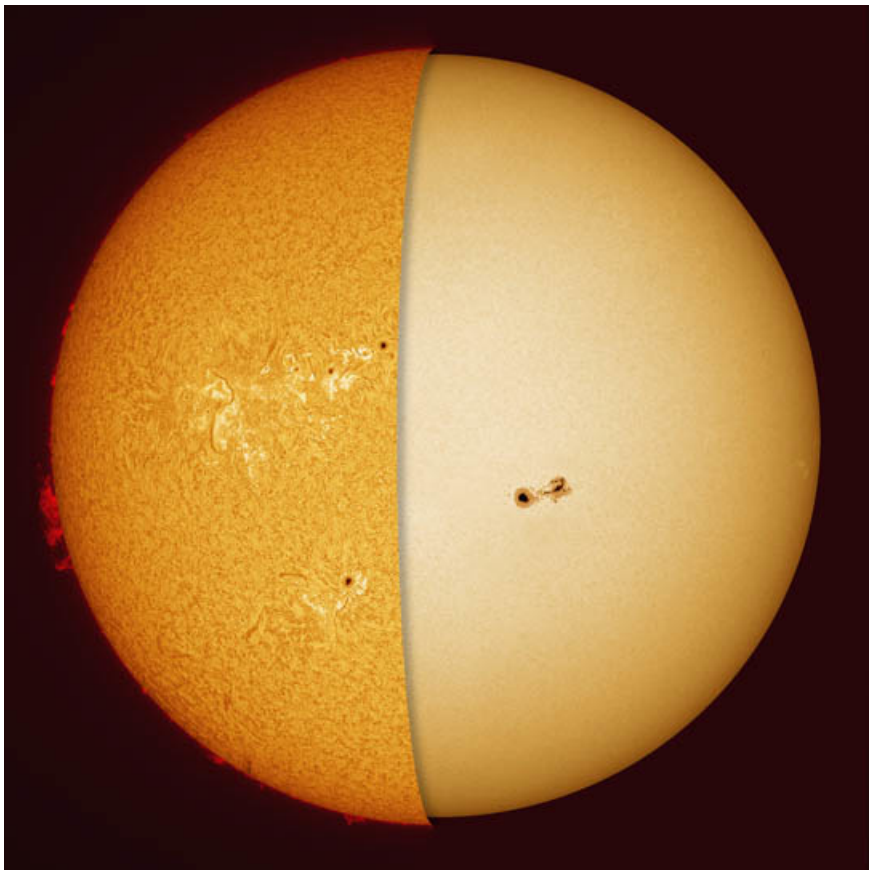

Figure 1.2: Sun in Hα (left) and in white light (right). Note the anatomy of spots in the photosphere, the dark penumbra surrounding the darker umbra. Also note the limb darkening on the photosphere. Alan Friedman, avertedimagination.com. Sky & Telescope.

1.4 Photometry & the Johnson-Cousins System

In the simplest terms, photometry is the measure of the brightness of an astronomical object. In the second century B.C, ancient Greek astronomer Hipparchus classified stars into six ranks based on their apparent brightness, with higher numbers (ranks) representing fainter stars. In 1856, Norman Pogson put photometry on a firmer mathematical footing by defining 5 steps on the magnitude scale as equivalent to a factor of 100 in brightness. Apparent magnitude is a measure of brightness as observed from Earth, and absolute magnitude is how bright a star would appear at a distance of 10 parsecs.

One way to dissect the broad spectrum of a star's electromagnetic output is to put colored filters in the optical path of a telescope, allowing a smaller but still broad (hundreds of nanometers wide) range of wavelengths to pass through. A widely-used system of colored

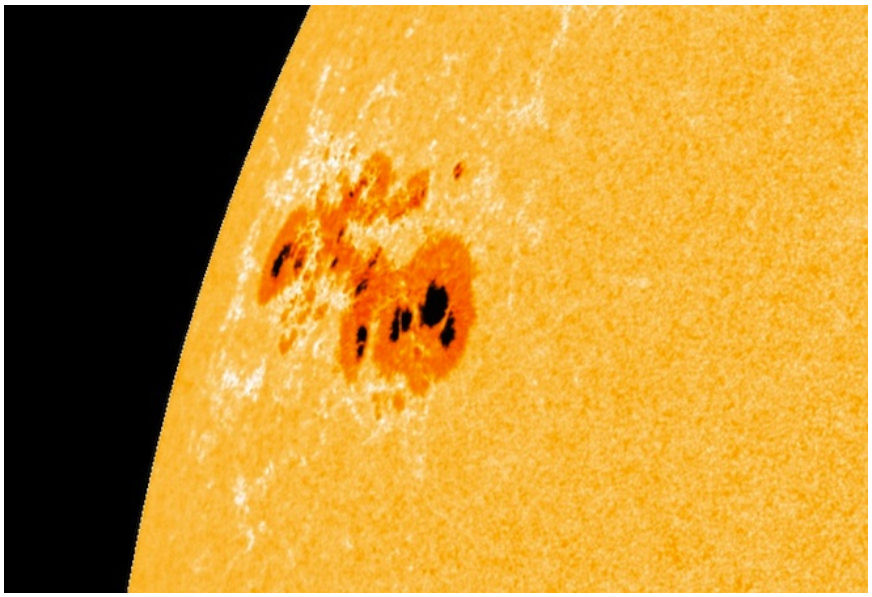

Figure 1.3: A detailed view of a sunspot near the solar limb. Note the dark umbra, lighter penumbra, and bright faculae. Image: NASA / SDO.

filters is the Johnson-Cousins system of U (ultraviolet), B (blue), V (visual), R (red), and I (infrared). Tracking a star's brightness through multicolor photometry reveals information about the color of the star, leading to information about the temperature. A plot of a star's photometry over time is known as a light curve.

A robotic observatory at DSO using a 300mm f/4 Pentax telephoto lens coupled with a Fingerlakes CCD employing a 4096 × 4096 pixel KAF-16803 chip has been monitoring the YSA program stars in Johnson-Cousins B, V, and R, as well as other bands. Using a novel photometric technique of adding up the flux from the other stars in the field to use as a comparison "super" star to provide a flux normalization. This system has been able to reduce photometric error to between 0.005 - 0.007 mag [10].

1.5 Stellar Spectral Classification

Edward C. Pickering began an all-sky survey of stellar spectra in the 1880's by equipping a camera with a thin prism mounted in front of the camera lens. Such an "objective prism" setup produces photographic images containing spectra of all the stars in the field of view. Williamina Fleming used the letters A – Q to classify stars based on the strength of the

hydrogen lines in the spectra. In 1901, Annie Jump Cannon changed the Fleming / Maury system by dropping all letter designations but O, B, A, F, G, K, and M, with the order now reflective of photospheric temperature. She also created a decimal system, adding a number after the letter, designating the sub-type (for example, spectra halfway between B and A were designated B5). The modern Morgan-Keenan classification system kept Cannon's spectral classes and added originally five, now seven, luminosity classes: 0 - hypergiant, Ia - bright supergiant, Ib - supergiant, II - bright giant, III - giant, IV - subgiant, and V - main sequence. This system is based on spectral line widths, which reveal photospheric pressure. The stars in the YSA sample are all young main sequence.

Stars are frequently referred to as "early" or "late." These relative terms are a holdover from a time when stellar evolution was thought to involve stars cooling over time while on the main sequence. "Early" stars are hotter, and "late" stars are cooler. The YSA sample is from late F to early K (F8 to K2). The Sun is a G2 V. HD 13531, the star used as a case study in this project, is a G7 V.

The 0.8 m Ritchey-Chrétien telescope at DSO has been collecting spectra for the YSA program stars using the GM spectrograph employing a 1200 g mm^{-1} grating. This combination gives a spectral range of 3800 – 4600 Å and a resolution of 1.8 Å/2 pixels.

1.6 Spectroscopic Indices

The evidence of a magnetically active star manifests in enhanced Far UV, Extreme UV, and X-ray emissions driven by magnetic heating. Fortunately for life on Earth, but unfortunately for our study, the Earth's atmosphere blocks these wavelengths prohibiting ground-based monitoring. A ground-based proxy is available to moderate-sized ground-based telescopes. Chromospheric flux in the Ca II H & K lines correlate with both Far UV and X-ray fluxes [12].

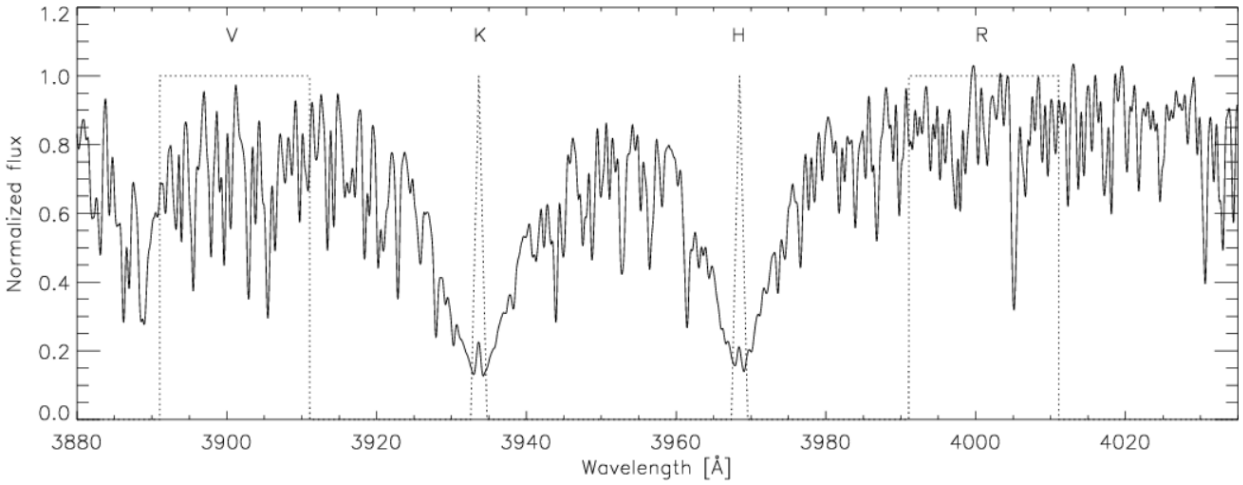

Figure 1.4: This normalized Fiber-fed Extended Range Optical Spectrograph (FEROS) spectrum of the slowly rotating F7 V star HD 48676 serves as a demonstration of the emission in the cores of the Ca II H & K lines. The H & K transmission bands employed by the Mount Wilson program are shown (dotted lines) as well as the red (R) and violet (V) "continuum" bands. The H & K transmission bands isolate the chromospheric emission in the cores of the broad Ca II H & K lines. Image from Schröder, Reiners, and Schmitt 2009 [20].

1.6.1 Chromospheric Index: The Ca II H & K index (S_{MW})

Ca II is the primary ionization stage of calcium in the photospheres and lower chromospheres of F-, G-, and K-type dwarfs. The Ca II H & K absorption lines show emission cores that arise from emission in the chromosphere, as seen in Figure 1.4.

The ratio of emission in the cores of Ca II H & K lines against the flux in the continuum on either side of the pair of lines is known as the Mount Wilson chromospheric activity index and is the standard measure of chromospheric activity in a star. The HK Project at the Mount Wilson Observatory regularly monitored the Ca II H & K emission of over 100 stars starting in 1966, and was the first project to characterize long-term magnetic variations of stars similar in nature to our Sun's 11 year cycle [21]. This 30 year long program is the foundation of our understanding of the link between magnetic activity and fundamental stellar properties. The HK Project found that older stars either vary in a smooth cyclic fashion or maintain steady levels of Ca II emissions, while younger stars vary strongly and irregularly. Baliunas et. al (1995) continued monitoring of the Mount Wilson stars and further strengthened the link between changes in stellar activity and Ca II H & K emissions [1].

The Mount Wilson S index is calculated by

$$S_{\mathrm{MW}} = \frac{\alpha(N_H + N_K)}{(N_R + N_V)} \tag{1.4}$$

where $(N_H + N_K)$ is the sum of the flux in the cores of the H & K lines, $(N_R + N_V)$ is the sum of the flux in the red and violet continua, and α is a calibration factor.

1.6.2 Photospheric Indices

Gray et al. developed three spectroscopic indices based on photospheric absorption features in the blue-violet region monitored by the DSO: G-band, Ca I, and Hγ [10]. These bands were chosen because they show different temperature sensitivities (Figure 1.5), and, under the hypothesis that they and their correlations with variations in the Johnson-Cousins bands, could be used to track the spot and facular coverage of a star.

Gray et al. hypothesized that temperature would be the "driving factor of changes in the photospheric indices [10]." However, their results showed all three spectroscopic indices showed anti-correlations with the chromospheric activity as measured by S_{MW}, and that all three indices showed strong direct correlations with each other. Gray et al. thus concluded that the variations shown by these indices "were not consistent with the hypothesis that the photospheric indices are primarily affected by temperature changes in the photosphere arising from changes in spots and photospheric faculae."

Gray et al. goes on to reference Basri et al. (1989) for mechanisms that may be relevant, including "continuum emission arising in the chromosphere or upper photosphere leading to the phenomenon of veiling," or "nonradiative heating in the upper layers of the photosphere in plage regions resulting in weaker line cores [2]." These were observed in certain active stars and caused the reduction of the equivalent widths of metallic lines (especially low-excitation lines) in the blue-violet part of the spectrum.

The photospheric model in this paper drives the photospheric indices by temperature alone. If this project can reproduce the observed relationships between the Johnson-Cousins B, V, and R photometry and the photospheric indices, then the original hypothesis in Gray et al. would be verified. If, however, the observed relationships cannot be reproduced, the

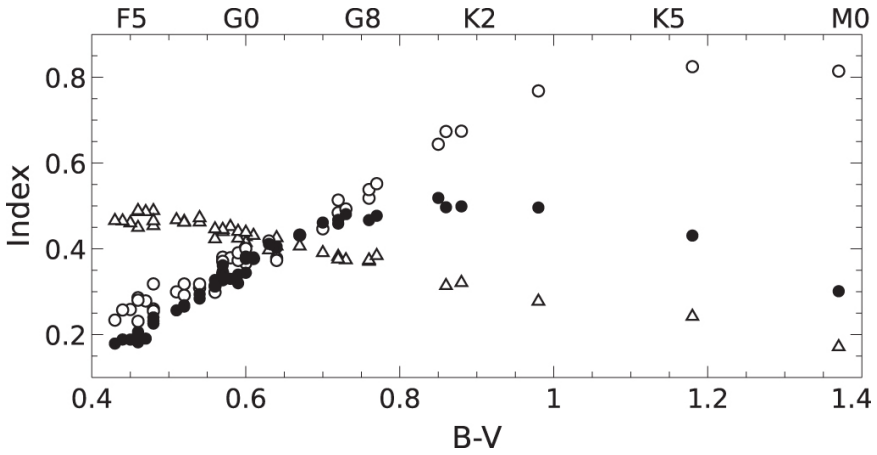

Figure 1.5: The photospheric indices as a function of $B-V$ color. Over the range of stars in the Gray et al. 2015 paper (F8 to K2), all three indices are linear. The G-band (solid circles) and Ca I (open circles) indices increase with with increasing $B-V$, while the Hγ index (open triangles) decreases linearly with increasing $B-V$. The stars in this sample are Mount Wilson calibration stars of Gray et al. (2003) [9] and the $B-V$ data are from Mermilliod et al (1997)[16]. Figure is from Gray et al. (2015) [10]

assertions of additional physics needed to describe the non-thermal effects (Basri et al.) would be strengthened.

The G-band Index

The G-band is a spectroscopic absorption feature in the blue-violet part of the spectrum arising from the 0-0 and 1-1 bands of the CH molecule ([11], [8]). Gray et al. defines the G-band index by integrating over a 14 angstrom-wide region characterizing the G-band absorption, then dividing by the fluxes in two continuum regions. The index is 0 when the G-band is absent (no absorption at all) and 1 when it is perfectly black.

$$\mathrm{G} = 1 - \frac{\frac{1}{14\mathring{A}} \int_{4298\mathring{A}}^{4312\mathring{A}} I(\lambda) d\lambda}{0.247 c_3 + 0.753 c_4} \tag{1.5}$$

The Ca I Index

The Ca I index was constructed similarly to the G-band index. It is also an absorption feature in the blue - violet spectrum and increases in strength with increasing spectral class [10].

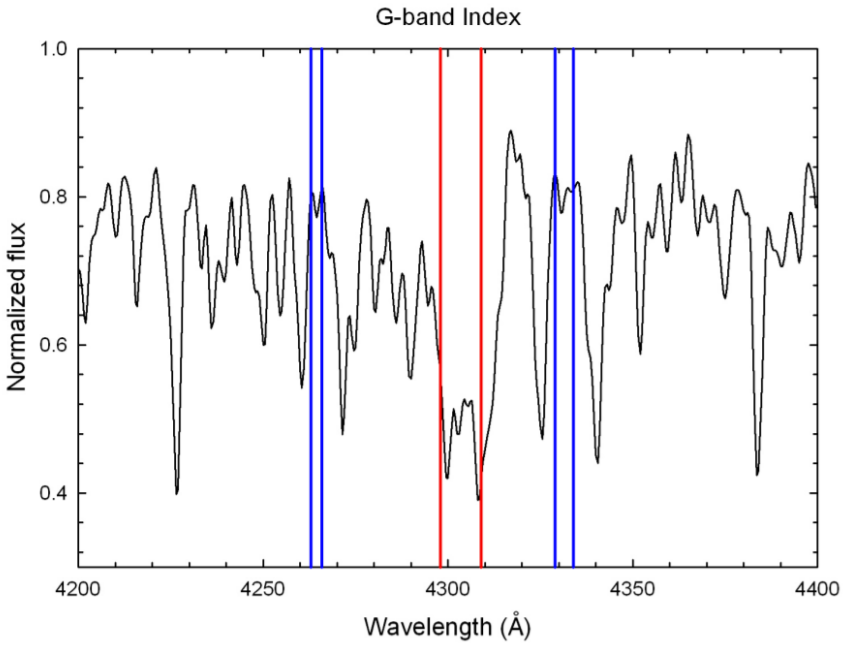

Figure 1.6: The photospheric G-band feature (red), with continua (blue). Image from Saken et al. (2015) [19]

$$\text{Ca I} = 1 - \frac{\frac{1}{2\mathring{A}} \int_{4225.7\mathring{A}}^{4227.7\mathring{A}} I(\lambda) d\lambda}{0.5(c_3 + c_4)} \tag{1.6}$$

The Hγ Index

A third index was constructed for the Hγ line. Gray et al. notes that it appear to have only about half the temperature sensitivity as the Ca I index.

$$\text{H}\gamma = 1 - \frac{\frac{1}{2\mathring{A}} \int_{4339.5\mathring{A}}^{4341.5\mathring{A}} I(\lambda) d\lambda}{0.4268c_3 + 0.5714c_4} \tag{1.7}$$

1.7 A Case Study: HD 13531

One of the YSA program stars, HD 13531 (also designated HIP 10339, V451 And), was chosen for closer study because early results showed it was brightest when the spot was transiting the star, suggesting facular dominance. Data from the 2017 observing season are shown in Figures 1.8 and 1.9, revealing that DSO's derivation of the Mount Wilson S index (S_2) is at

Table 1.1: Band definitions for the photospheric indices ([10]).

Band Name	Violet Edge	Red Edge
Continuum (c_1)	4208.0 Å	4214.0 Å
Ca I	4225.7 Å	4227.7 Å
Continuum (c_2)	4239.4 Å	4245.4 Å
Continuum (c_3)	4263.0 Å	4263.0 Å
G-band	4298.0 Å	4312.0 Å
Continuum (c_4)	4316.0 Å	4320.5 Å
Continuum (c_5)	4329.0 Å	4334.0 Å
Hγ	4339.5 Å	4341.5 Å
Continuum (c_6)	4345.0 Å	4349.5 Å

its maximum when the Johnson-Cousins B, V, and R magnitudes are at their minima. This means the star is dimmest when the spot transits the star. Table 1.2 shows the observed modulations for HD 13531 during the 2017 observing season at DSO. It is these modulations that the CHEETAH code (Section 2.5) attempts to fit by changing the characteristics of the spot. While five of the signals showed strong periodicity at $P = 7.45$ days, Hγ did not, even though it did show variations greater than expected from the measurement errors (Richard O. Gray, personal communication).

Table 1.2: Observed modulations for HD 13531

Index	Amplitude of Modulation
B	0.028
V	0.020
R	0.018
G-band	0.00268
Hγ	0.00390
Ca I	0.00788

1.8 Model Photospheres and Their Assumptions

Model photospheres are not an elementary exercise. The usual simplifications in modelling photospheres assume plane parallel geometry and hydrostatic equilibrium, and neglect

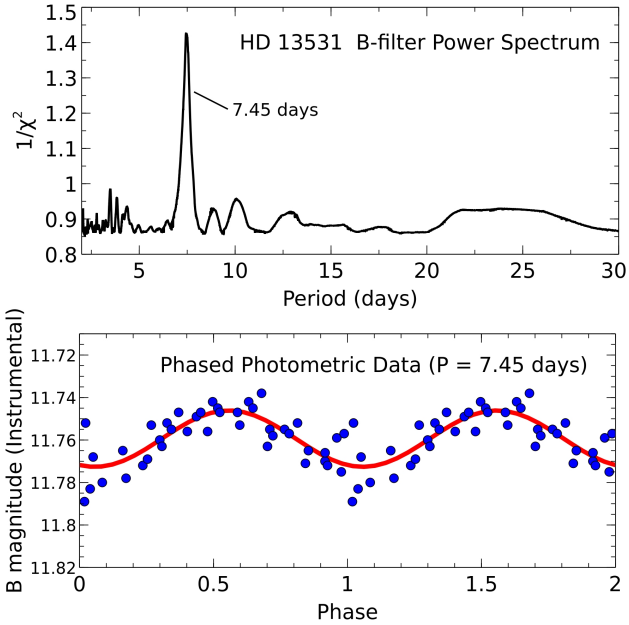

Figure 1.7: B power spectrum and phased B photometric data for HD 13531 during the 2017 observing season. Richard O. Gray.

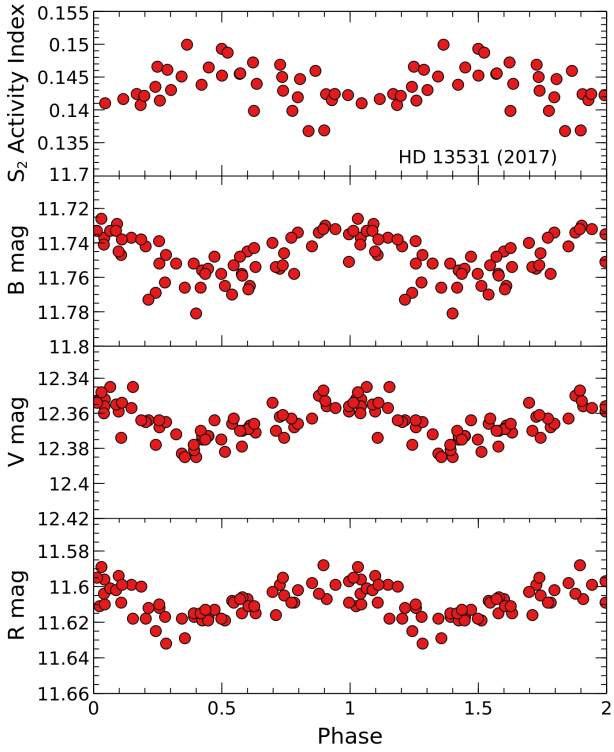

Figure 1.8: Johnson-Cousins B, V, and R photometry and S_{MW} index for HD 13531 during the 2017 observing season. Richard O. Gray.

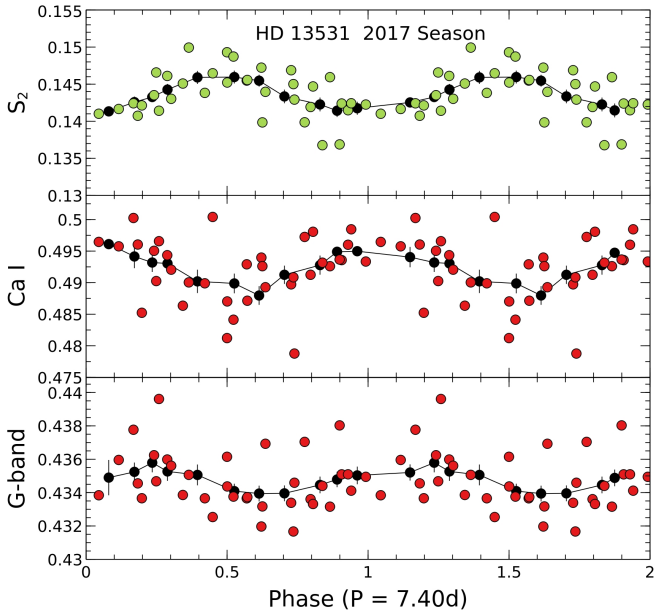

Figure 1.9: DSO's derived Mount Wilson index S_2 and the G-band and Ca I indices for HD 13531 during the 2017 observing season. Hγ index did not show periodicity at P = 7.45 days and has been excluded. Richard O. Gray.

granulation, spots, and magnetic fields [6]. The models used in this project (Section 2.1) assume local thermodynamic equilibrium, hydrostatic equilibrium, and a plane-parallel atmosphere.

Assuming local thermodynamic equilibrium for a local computational volume makes the following simplifications. The radiation incident on the volume is the blackbody spectrum described by Planck's radiation law, set only by the local temperature:

$$I_\nu = \frac{2h\nu^3}{c^2} \frac{1}{e^{\frac{h\nu}{kT}} - 1} \tag{1.8}$$

where I_ν is the intensity of radiation as a function of frequency ν, h is Planck's constant, c is the speed of light, k is the Boltzmann constant, and T is the temperature of the volume.

The relative number of atoms with electrons occupying different excited energy states is determined by the Boltzmann equation, set by the electron's excitation energies and the local temperature:

$$\frac{n_2}{n_1} = \frac{g_2}{g_1} \exp\left(-\frac{\Delta \mathrm{E}}{\mathrm{kT}}\right) \tag{1.9}$$

where n_2 and n_1 are the number density of atoms with electrons in levels 1 and 2, g_1 and g_2 are the statistical weights of the first and second energy level, ΔE is the energy difference between the two levels, k is the Boltzmann's constant and T is the local kinetic temperature.

The proportion of atoms in different ionization states is set by the Saha equation, set by the atomic ionization energy and the local temperature:

$$\frac{N_1}{N_0} = \frac{(2\pi m_e)^{3/2}(kT)^{5/2}}{P_e h^3} \frac{2u_1(T)}{u_0(T)} e^{-I/kT} \tag{1.10}$$

where N_1/N_0 is the ratio of ions to neutrals, $u_1(T)/u_0(T)$ is the ratio of ionic to neutral partition functions, m_e is the electron mass, P_e is the pressure due to free electrons in the ionized gas of the photosphere, and I is the ionization potential.

Chapter 2

Methods

2.1 ATLAS9 Models

ATLAS9 stellar atmosphere models are generated with the ATLAS9 program [4]. These models assume local thermodynamic equilibrium (LTE), hydrostatic equilibrium, and plane parallel symmetry. The file header for each model lists the effective temperature, specific gravity (log(g)), metallicity (M/H), and number of layers. The columns are mass depth, temperature, gas pressure, electron density, Rosseland mean absorption coefficient, radiation pressure, and microturbulent velocity.

```
5777.0  4.43770  0.00  64
2.62383508E-03   3398.7 7.188E+01 6.618E+09 7.359E-04 1.133E-01 1.500E+05
2.62384162E-03   3871.5 7.188E+01 1.301E+10 7.359E-04 8.267E-02 1.500E+05
3.17880896E-03   3901.4 8.709E+01 1.566E+10 8.502E-04 7.839E-02 1.500E+05
4.02509434E-03   3937.8 1.103E+02 1.966E+10 1.019E-03 7.581E-02 1.500E+05
4.97406188E-03   3969.0 1.363E+02 2.409E+10 1.202E-03 7.460E-02 1.500E+05
```

Figure 2.1: The header and first five layers of the ATLAS9 model for the Sun.

2.2 SPECTRUM

SPECTRUM is a stellar spectral synthesis code which computes the emergent stellar spectrum using ATLAS9 or similar stellar atmosphere models [7]. It is suitable for

the computation of synthetic stellar spectra for stars from spectral type B to early M. SPECTRUM uses three columns of data from the ATLAS9 models: mass depth, temperature, and gas pressure. The program then calculates the electron number densities and the number densities of numerous species, their ions, and diatomic molecules by solving a system of nonlinear equilibrium equations. The total number densities of all species must agree with $P_{\rm gas}/kT$ from the ATLAS9 models. The program then computes the reference opacities and optical depths at each level and, finally, the synthetic spectrum using a spectral line list consisting of data for hundreds of thousands of atomic and molecular transitions.

Among SPECTRUM's output modes are the ability to generate an integrated flux spectrum, a normalized spectrum, and a specific intensity mode which requires an input of μ, the direction cosine.

2.3 Mgrid

Mgrid is a library of specific intensity spectra computed using SPECTRUM for a range of effective temperatures ($T_{\rm eff}$) from 4000 to 6500 K in 100 K increments and $\log g$ (surface gravity) values of 4.0, 4.5, and 5.0. For each combination of effective temperature and $\log g$, specific intensity spectra were computed at 9 different values of $\mu = \hat{\mathbf{s}} \cdot \hat{\mathbf{n}} = \cos\theta$ where $\hat{\mathbf{n}}$ is the normal to the top of the photosphere, and $\hat{\mathbf{s}}$ is the direction along the line of sight. The BlankHD and CHEETAH programs (explained below) interpolate in the 3-D ($T_{\rm eff}$, $\log g$, and μ) Mgrid library to obtain the required specific intensity spectrum for each gridpoint on the stellar surface. Since the YSA project deals with young Population I stars, solar abundances were used for the Mgrid spectra computations. The microturbulent velocity (the non-thermal component of gas velocity, a source of spectral line broadening) used in these calculations was 1 km/s.

2.4 BlankHD

Since most of the star will be the same effective temperature, running the same interpolation routines for temperature and log(g) on every grid point is computationally inefficient.

BlankHD is a program that calculates the spectrum of each grid point on a 50 x 50 array representing a quadrant of a spotless 100 x 100 star with a particular effective temperature and specific gravity. The Mgrid library of spectra from SPECTRUM are read into blankHD and are weighted by interpolation routines based on temperature and specific gravity, then again by limb darkening and geometric effects due to the grid points location on the disk of the star. A spectrum for each grid point was computed and stored in order to be referenced by CHEETAH.

2.5 CHEETAH

The CHromosphere Excluded Exercise in The Analysis of pHotospheres, or CHEETAH, simulates rotational modulation of a star by modelling the transit of a spot with umbra, penumbra, and faculae across a stellar disk, then calculates light curves of the photometric flux of a star in Johnson B, V, and R band passes as well as calculating the G-band, Hγ, and Ca I indices.

CHEETAH establishes the parameters of a spot with the following temperatures: $T_{\rm eff}$ = 5595.0, $T_{\rm umbra}$ = 4000.0, $T_{\rm penumbra}$ = 5295.0, $T_{\rm facula}$ = 5695.0 or 5895.0. The facula filling factor $d_{\rm fac}$ is 1.0 for the "solid halo" model and 0.3 for the "sprinkled in" faculae. Spot radii $R_{\rm umbra}$, $R_{\rm penumbra}$, and $R_{\rm facula}$ are optimized using Powell's method (Section 2.8).

The program then goes through each pixel of a 100 by 100 pixel array. At each pixel, the arc length from the spot center is calculated. If the arc length is less than the radius of the umbra, then the temperature of that point is assigned as T_{umbra}. Else, if the arc length is less than the radius of the penumbra, then the temperature is $T_{penumbra}$. Else if the arc length is less than the radius of the faculae radius, and a random number between 0 and 1 is less than or equal to the faculae filling factor, then the temperature is $T_{\rm facula}$. Else, the temperature is $T_{\rm eff}$.

With the preliminaries dispensed with, CHEETAH determines the specific intensity from this pixel. If the temperature of the pixel is the effective temperature, the program pulls in the appropriate blankHD spectrum, taking into account symmetry. The blankHD spectrum is added to the flux file for that rotation, for each of the 27,500 wavelengths.

If however the temperature for that pixel is not the effective temperature, the program carries out 3-D interpolation in the Mgrid library to obtain a specific intensity spectrum for the temperature, surface gravity, and direction cosine of the pixel. The resultant spectrum is added to the flux for that rotation, again looping through each of the 27,500 discrete wavelengths.

After having looped through the entire 100 x 100 array representing the stellar disk, the B, V, and R fluxes are computed, as well as the G-band, Hγ, and Ca I indices for that rotation state of the star. The program compares the index for that rotation state to the maximum and minimum for each of the six signals, and if the current index is more extreme than either, then it becomes the new extreme. The longitude for the max or min is also recorded.

The longitude of the spot is incremented by $\frac{\pi}{25}$ radians and the process repeats until the spot has made a full revolution. Then, the modulation is calculated for each index, subtracting the minimum from the maximum for the photometric fluxes and maximum from minimum for the spectroscopic indices. If the spot is on the back of the star when a maximum value occurs, then that modulation is made to be negative.

With a list of synthetic modulations now in hand, the program loops through the six bands and calculates a weighted error value comparing them to the observed modulations. The photometric fluxes were assigned a weight of 1 and the spectroscopic indices a weight of 0. The error is calculated by

$$\chi^2 = \sum_{i=1}^{6} \frac{w_i(syn_i - obs_i)^2}{obs_i} \tag{2.1}$$

where χ^2 is the error, w_i is the weight, syn_i is the synthetic modulation in that band, and obs_i is the observed modulation of that band. The error value is reported to the Powell's method routine, described in section 2.8.

2.6 Stellar Surface Integration

Both BlankHD and CHEETAH use the following method to integrate over the stellar surface to derive the flux from the star:

$$F_\lambda = \int I_\lambda \; \mu \; d\Omega = \int I_\lambda \; \cos\theta \; \sin\theta \; d\theta \; d\phi$$

where F_λ is the integrated monochromatic flux, and I_λ is the monochromatic specific intensity for direction μ, and μ the direction cosine at a given pixel on the stellar disk.

The integral is over the entire visible hemisphere of the star in the CHEETAH program, and over one quadrant of the visible hemisphere in the BlankHD program. The numerical integration is carried out with Gaussian quadrature, with Gauss-Legendre integration along the θ direction, and Gauss-Chebyshev integration along the ϕ direction. This integral is carried out at 27,500 wavelengths, from 3500 – 9000Å, with a wavelength step of 0.2Å.

2.7 Model Parameters

2.7.1 Faculae

In other studies that have modeled spots with faculae, the facular region has been modeled as a solid halo with a temperature 100 K above the effective temperature [5]. Since photographs of the active Sun show faculae are dispersed somewhat randomly near spots rather than a solid ring, we included faculae at +300 K placed with a filling factor of 0.3 in a halo around the penumbra. The faculae placement is determined by comparing a random number between 0 and 1, generated by rand() in C, to the facula filling factor, $d_{\rm fac}$. If the random number is less than the faculae filling factor, the pixel is designated as facula.

2.7.2 Umbra & Penumbra

The umbra was modeled at 4000 K, or about 1600 K cooler than the effective temperature. The penumbra was modelled at 5295 K, or 300 K cooler than the effective temperature. At a resolution of 100 x 100, each gridpoint comprises 1/10,000 or 0.01% of the stellar disk.

A common characterization of active region size on the Sun is millionths of a heliosphere (visible disk of the sun), or MH. Each gridpoint represents a spot size of 100 MH. Large spots on the sun can be as large as 2000 MH.

2.8 Powell's Method, Error Minimization

A modified Numerical Recipes [18] version of Powell's method calls the CHEETAH program as a function. It adjusts the size of the umbra, penumbra, and faculae to minimize a error value calculated against the observed modulations of HD 13531.

2.9 Summary of Workflow

- ATLAS9 model gives mass depth, temperature, and gas pressure for 64 layers of a plane-parallel photosphere
- SPECTRUM calculates synthetic emergent spectra including
  - temperature from 4000 to 6500 K, every 100 K
  - surface gravity (log g) of 4.0, 4.5, and 5.0 dex
  - direction cosine (μ) values of 1.000e-4, 3.162e-4, 1.000e-3, 3.162e-3 ,1.000e-2, 3.162e-2, 1.000e-1, 3.162e-1, and 1.
- A library of spectra organized by temperature, specific gravity, and direction cosine values, called Mgrid, is compiled.
- A library of non-spot spectra is made by calling on Mgrid, calculating the specific intensity spectrum contributed by each grid point of a quadrant of a spotless star.
- For each rotation state, CHEETAH models a stellar disk with a spot. Then the program computes the flux spectrum for the entire disk, calculates the Johnson B, V, and R fluxes and G-band, Hγ, and Ca I indices, then rotates the star by incrementing the longitude of the spot by $\frac{\pi}{25}$ radians and repeats for a full revolution of the star.

- An error value comparing the synthetic modulations to the observed modulations is calculated and returned.
- Powell's method routine changes umbra, penumbra, and facula radii and repeats until a minimum error value is found.

Chapter 3

Results

3.1 Chi-squared Minimized Spot Size

Results from the "Solid Halo" and "Sprinkled In" models are shown in Tables 3.1 and 3.2. $T_{\rm fac}$ is the temperature added above $T_{\rm eff}$ to the faculae, and $d_{\rm fac}$ is the facular filling factor. $R_{\rm umbra}$, $R_{\rm penumbra}$, and $R_{\rm facula}$ are the radii of the umbra, penumbra, and facula regions, respectively, measured in radians. The B, V, R, G-band, Hγ, and Ca I columns list the modulations in those indices. Finally, the χ^2 value comparing the synthesized modulations to the observed modulations for that run is shown.

3.2 Synthetic Light Curves

Light curves for the "Solid Halo" and "Sprinkled In" models in Johnson-Cousins B, V, and R bands are shown in Figures 3.1, 3.2, and 3.3, while the plots of the G-band, Hγ, and Ca I indices are shown in Figures 3.4, 3.5, and 3.6. The horizontal axis in each plot shows the longitude of the spot in radians. These plots show the magnitudes and index values for a star with a spot starting on the back of the star and rotating one full revolution. The properties of the spot are those from Table 3.1.

Table 3.1: Model temperature, facula filling factor and best fit spot sizes (radians).

Model	$T_{\rm fac}$	$d_{\rm fac}$	$R_{\rm umbra}$	$R_{\rm penumbra}$	$R_{\rm facula}$
"Solid Halo"	+100 K	1.0	0.126	0.141	0.190
"Sprinkled in"	+300 K	0.3	0.133	0.146	0.194

Table 3.2: Synthesized modulations for HD 13531

Model	B	V	R	G-band	Hγ	Ca I	χ^2
Observed	0.028	0.020	0.018	0.00268	0.00788	0.00370	
"Solid Halo"	0.023	0.021	0.019	0.00105	0.00189	0.00110	0.000997
"Sprinkled in"	0.026	0.023	0.021	0.00129	0.00242	0.00131	0.001081

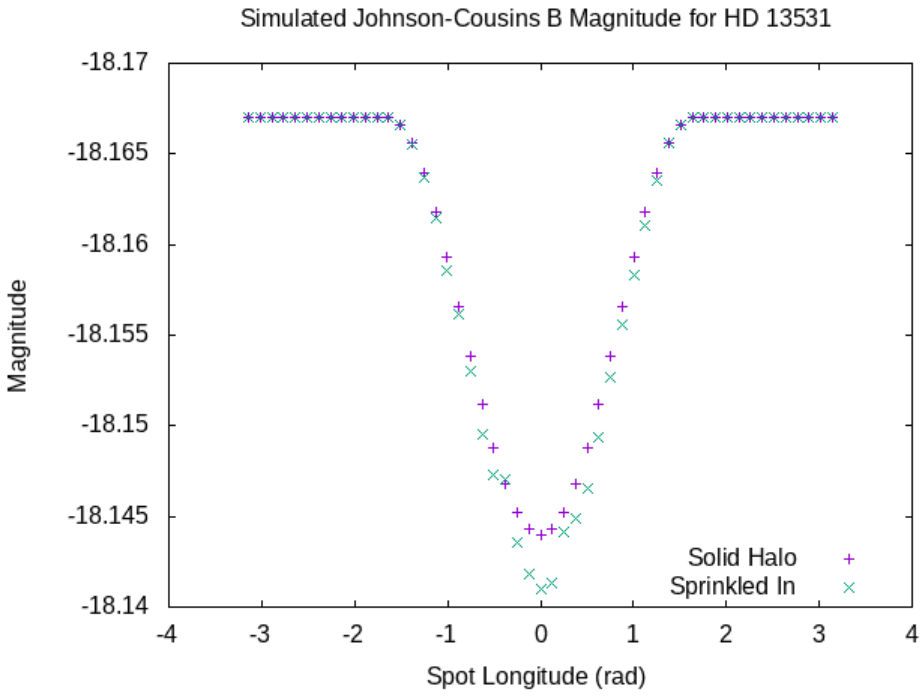

Figure 3.1: Johnson-Cousins B magnitude for "Solid Halo" and "Sprinkled In" Models.

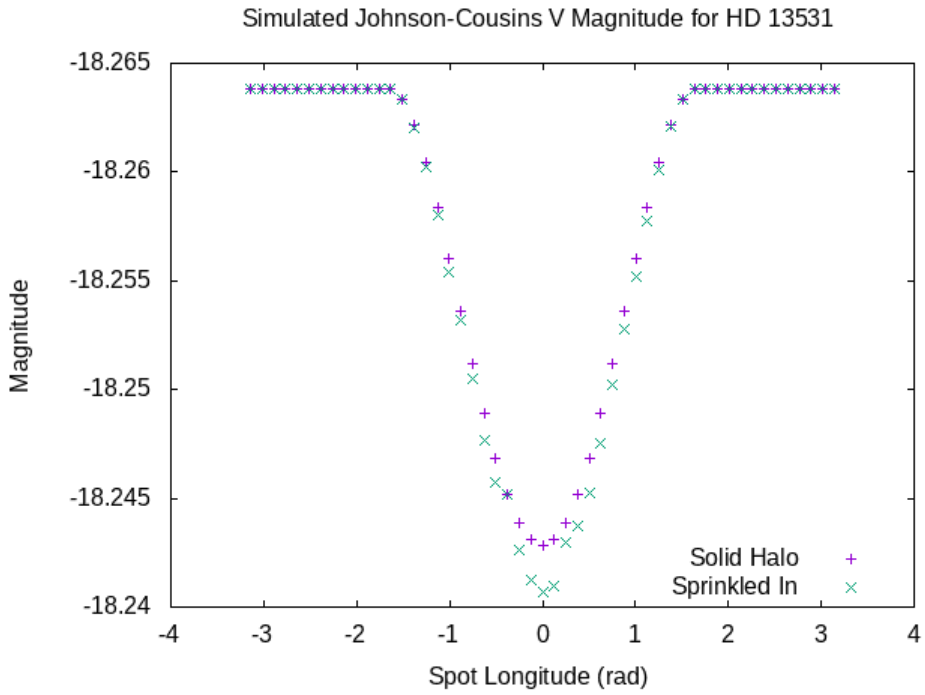

Figure 3.2: Johnson-Cousins V magnitude for "Solid Halo" and "Sprinkled In" Models.

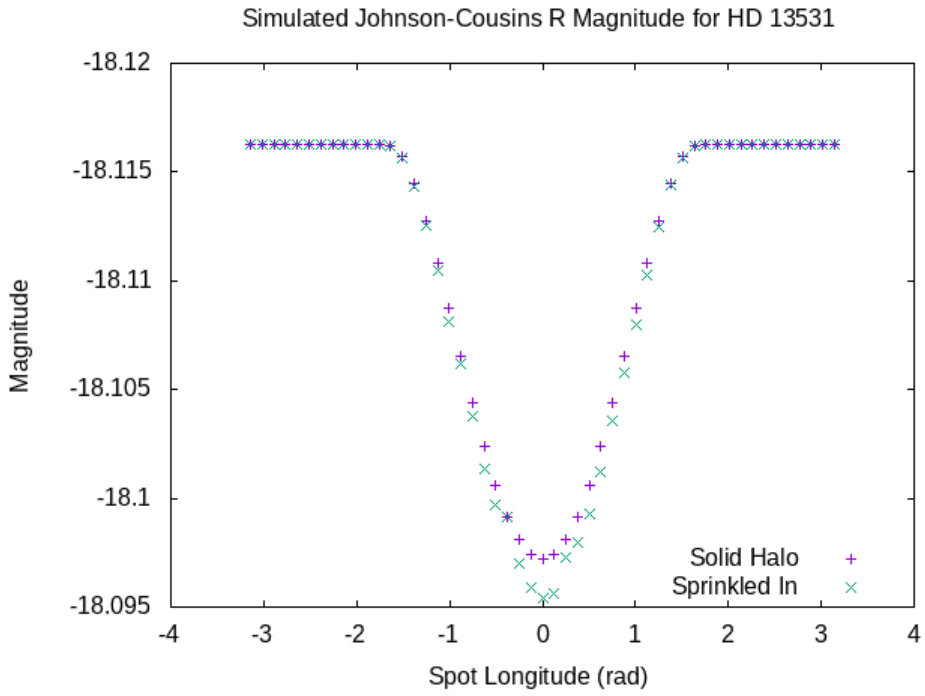

Figure 3.3: Johnson-Cousins R magnitude for "Solid Halo" and "Sprinkled In" Models.

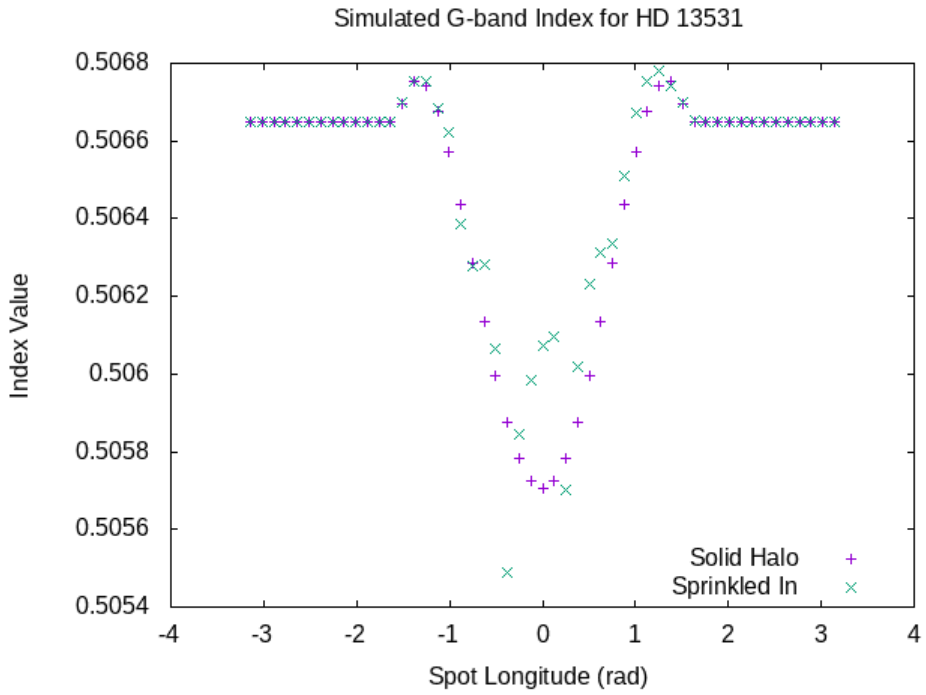

Figure 3.4: G-band index for "Solid Halo" and "Sprinkled In" models.

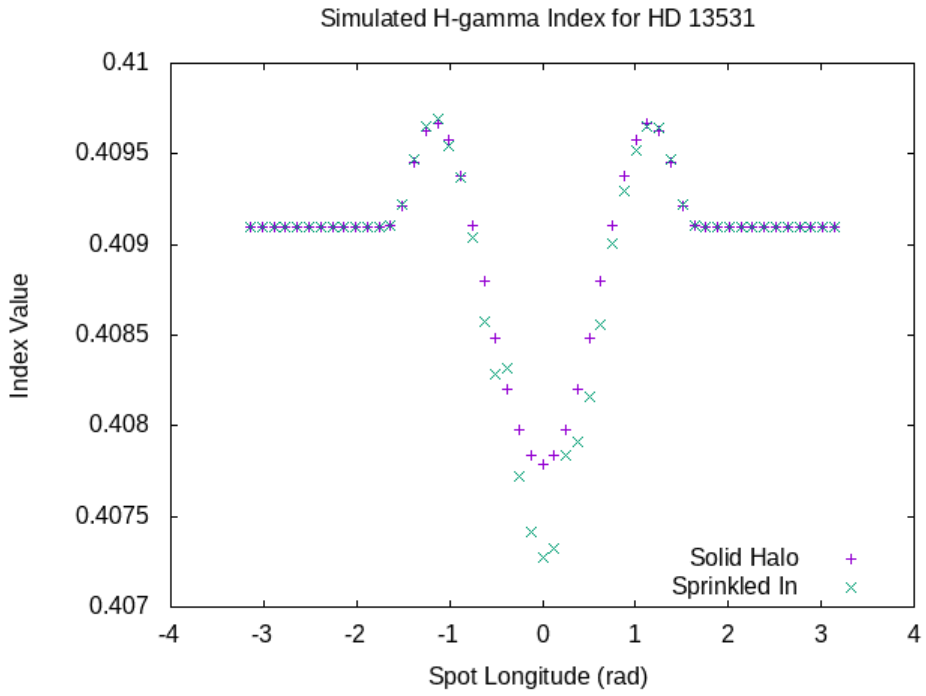

Figure 3.5: Hγ index for "Solid Halo" and "Sprinkled In" models.

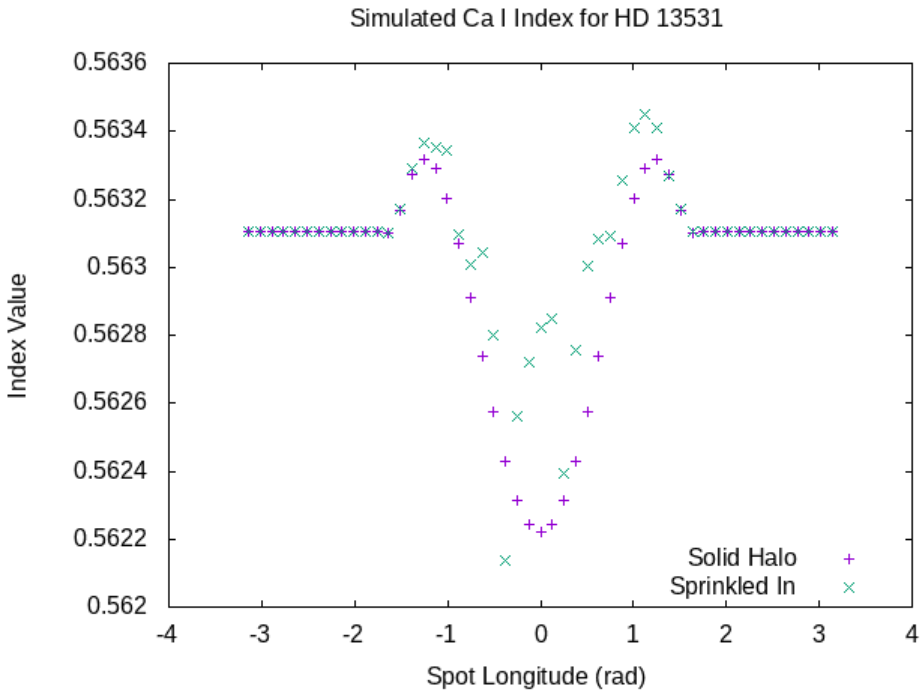

Figure 3.6: Ca I index for "Solid Halo" and "Sprinkled In" models.

Chapter 4

Conclusions

4.1 Light Curves & Modulations

Both models' best fit photometry results in modulations in the spectroscopic indices that are too small by factors of between 2.0 and 4.2. Modelling faculae of +300 K randomly painted in with a filling factor of 0.3, rather than a solid halo of +100, increases the synthetic modulation to about half of the observed. Hence it appears from these preliminary calculations that we cannot explain the behavior of the spectroscopic indices on temperature variations alone. This evidence supports the conclusions from Gray et al., regarding non-thermal mechanisms (Basri et al.). Both models show that the spectroscopic indices are more sensitive to temperature changes in the stellar disk than the photometric flux, in agreement with Lockwood et al. [13].

4.2 Synthetic Light Curve Shape

As seen in Figure 1.8, the observed light curves are sinusoidal. A single spot is used in the model curves and produces a U-shaped dip rather than a sinusoidal curve. A pair of spots comprising an active latitude could produce a sinusoidal light curve. This would result in the chromospheric activity period to be half as large as the star's rotation period found by doppler broadening (v sin i). Since we do not know the inclination, at best we can place a lower limit on the rotational speed, therefore an upper limit for the rotational period using

doppler broadening. For HD 13531, the light curve period is 7.45 days as measured by the DSO light curves, and Gray et al. found periods of 8.06 ± 2.37 days based on the R'_{HK} index ([17], [15]), and a maximum period based on doppler broadening (v sin i) of 7.38 ± 0.12. Therefore we know the photosphere of HD 13531 does not consist of a single spot, or of a pair of spots comprising an active latitude.

4.3 Future Work

The model photosphere method from this thesis shows promise for studies of spot and faculae coverage on stars. In specific regard to the YSA project, next steps to build from these preliminary calculations would include adding inclination, multiple spots at various latitudes, and differential rotation to the model to attempt to match the shape of the light curve rather than just the magnitude of rotational modulation. Allowing Powell's method to change faculae filling factor as well as the umbra, penumbra, and facula temperatures would allow for a closer match of the Johnson-Cousins B, V, and R photometry.

Bibliography

[1] Baliunas, S. L., Donahue, R. A., Soon, W. H., Horne, J. H., Frazer, J., Woodard-Eklund, L., Bradford, M., Rao, L. M., Wilson, O. C., Zhang, Q., Bennett, W., Briggs, J., Carroll, S. M., Duncan, D. K., Figueroa, D., Lanning, H. H., Misch, T., Mueller, J., Noyes, R. W., Poppe, D., Porter, A. C., Robinson, C. R., Russell, J., Shelton, J. C., Soyumer, T., Vaughan, A. H., and Whitney, J. H. (1995). Chromospheric variations in main-sequence stars. *The Astrophysical Journal*, 438:269–287, ISSN: 0004-637X, DOI: 10.1086/175072, http://adsabs.harvard.edu/abs/1995ApJ...438..269B. 10

[2] Basri, G., Wilcots, E., and Stout, N. (1989). Photospheric activity in main sequence stars. *Astronomical Society of the Pacific, Publications*, 101:528–540, DOI: 10.1086/132464. 11

[3] Berger, T. E., Title, A. M., Tarbell, T., Rouppe van der Voort, L., Lofdahl, M. G., and Scharmer, G. B. (2007). What are 'Faculae'? In Shibata, K., Nagata, S., and Sakurai, T., editors, *New Solar Physics with Solar-B Mission*, volume 369 of *Astronomical Society of the Pacific Conference Series*, page 103. 5

[4] Castelli, F. and Kurucz, R. L. (2004). New Grids of ATLAS9 Model Atmospheres. *ArXiv Astrophysics e-prints*, pages arXiv:astro–ph/0405087, http://adsabs.harvard.edu/abs/2004astro.ph..5087C. 18

[5] Gondoin, P. (2008). Contribution of Sun-like faculae to the light-curve modulation of young active dwarfs. *Astronomy and Astrophysics*, 478:883–887, DOI: 10.1051/0004-6361:20078245. 22

[6] Gray, D. F. (2005). *The Observation and Analysis of Stellar Photospheres*. Cambridge University Press. 15

[7] Gray, R. O. (2010). Documentation for Spectrum v2.76. http://www.appstate.edu/~grayro/spectrum/spectrum276.pdf. 18

[8] Gray, R. O. and Corbally, J., C. (2009). *Stellar Spectral Classification*. Princeton University Press. 12

[9] Gray, R. O., Corbally, C. J., Garrison, R. F., McFadden, M. T., and Robinson, P. E. (2003). Contributions to the Nearby Stars (NStars) Project: Spectroscopy of Stars Earlier

than M0 within 40 Parsecs: The Northern Sample. I. *The Astrophysical Journal*, 126:2048–2059, DOI: 10.1086/378365. ix, 12

[10] Gray, R. O., Saken, J. M., Corbally, C. J., Briley, M. M., Lambert, R. A., Fuller, V. A., Newsome, I. M., Seeds, M. F., and Kahvaz, Y. (2015). The Young Solar Analogs Project. I. Spectroscopic and Photometric Methods and Multi-year Timescale Spectroscopic Results. *The Astronomical Journal*, 150(6):203, ISSN: 1538-3881, DOI: 10.1088/0004-6256/150/6/203, http://stacks.iop.org/1538-3881/150/i=6/a=203. v, viii, ix, 1, 8, 11, 12, 14

[11] Hall, J. C. (2008). Stellar Chromospheric Activity. *Living Reviews in Solar Physics*, 5:2, DOI: 10.12942/lrsp-2008-2, http://adsabs.harvard.edu/abs/2008LRSP....5...2H. 6, 12

[12] Hempelmann, A., Schmitt, J. H. M. M., Baliunas, S. L., and Donahue, R. A. (2003). Evidence for coronal activity cycles on 61 Cygni A and B. *Astronomy and Astrophysics*, 406:L39–L42, ISSN: 0004-6361, DOI: 10.1051/0004-6361:20030882, http://adsabs.harvard.edu/abs/2003A%26A...406L..39H. 9

[13] Lockwood, G. W., Skiff, B. A., Henry, G. W., Henry, S., Radick, R. R., Baliunas, S. L., Donahue, R. A., and Soon, W. (2007). Patterns of Photometric and Chromospheric Variation among Sun-like Stars: A 20 Year Perspective. *The Astrophysical Journal Supplement Series*, 171:260–303, ISSN: 0067-0049, DOI: 10.1086/516752, http://adsabs.harvard.edu/abs/2007ApJS..171..260L. 6, 30

[14] Lockyer, J. N. (1868). Notice of an Observation of the Spectrum of a Solar Prominence, by J. N. Lockyer, Esq. *Proceedings of the Royal Society of London Series I*, 17:91–92. 6

[15] Mamajek, E. E. and Hillenbrand, L. A. (2008). Improved Age Estimation for Solar-Type Dwarfs Using Activity-Rotation Diagnostics. *The Astrophysical Journal*, 687:1264–1293, DOI: 10.1086/591785. 31

[16] Mermilliod, J.-C., Mermilliod, M., and Hauck, B. (1997). The General Catalogue of Photometric Data (GCPD). II. *A&A Supplement series*, 124:349–352, DOI: 10.1051/aas:1997197. ix, 12

[17] Noyes, R. W., Hartmann, L. W., Baliunas, S. L., Duncan, D. K., and Vaughan, A. H. (1984). Rotation, convection, and magnetic activity in lower main-sequence stars. *Astrophysical Journal*, 279:763–777, DOI: 10.1086/161945. 31

[18] Press, W. H., Flannery, B. P., and Teukolsky, S. A. (2007). *Numerical recipes. The art of scientific computing, 3rd Ed.* Cambridge: University Press, 2007. 23

[19] Saken, J. M., Gray, R. O., Corbally, C. J., and Briley, M. M. (2015). The Young Solar Analogs Project - Observations and Analysis. In van Belle, G. T. and Harris, H. C., editors, *18th Cambridge Workshop on Cool Stars, Stellar Systems, and the Sun*, volume 18 of *Cambridge Workshop on Cool Stars, Stellar Systems, and the Sun*, pages 131–136. ix, 13

[20] Schröder, C., Reiners, A., and Schmitt, J. H. M. M. (2009). Ca II HK emission in rapidly rotating stars. *Astronomy and Astrophysics*, 493:1099–1107. ix, 10

[21] Wilson, O. C. (1978). Chromospheric variations in main-sequence stars. *The Astrophysical Journal*, 226:379–396, ISSN: 0004-637X, DOI: 10.1086/156618, http://adsabs.harvard.edu/abs/1978ApJ...226..379W. 10

Vita

David McCallister is a proud native of Wayne County, WV. He has over a decade of experience in education and public outreach, in both formal classroom roles and informal settings like planetariums and star parties. He taught high school physics in Northern Kentucky for several years before moving to Knoxville, TN with his wife Sarah. He has a B.A. in Physics from Northern Kentucky University and a Master of Arts in Teaching from Thomas More College. David is an Astronomy Ambassador from the American Astronomical Society, and has been awarded the Wayne Kincaid Award and the Robert W. Lide Citation by the UT Physics and Astronomy Department for service to the astronomy laboratory and outreach programs.